Metabolic competency of larval zebrafish in drug-induced liver injury: a case study of acetaminophen poisoning

Yijia Chen[*], Weiyi Song[†], Wei Ge[†, 1], Ru Yan[*, ‡, 2]

[*]State Key Laboratory of Quality Research in Chinese Medicine, Institute of Chinese Medical Sciences, University of Macau, Taipa, Macao, China

[†]Center of Reproduction, Development and Aging (CRDA), Faculty of Health Sciences, University of Macau, Taipa, Macau, China

[‡]Zhuhai UM Science & Technology Research Institute, Zhuhai, 519080, China

[1] To whom correspondence should be addressed at Faculty of Health Sciences, University of Macau, Research Building N22, Taipa, Macau, China. Email: weige@um.edu.mo. https://orcid.org/0000-0002-4296-1585.

[2]To whom correspondence should be addressed at Institute of Chinese Medical Sciences, University of Macau, Research Building N22, Taipa, Macau, China. Email: ruyan@um.edu.mo. https://orcid.org/0000-0001-6268-360X.

Abstract

Larval zebrafish is emerging as a new model organism for studying drug-induced liver injury (DILI) with superiorities in visual assessment, genetic engineering as well as high throughput. Metabolic bioactivation to form reactive intermediates is a common event that triggers DILI. This study first addressed the correlation between acetaminophen metabolism and hepatotoxicity in zebrafish larvae (3 days post-fertilization) and demonstrated the occurrence of cytochrome P450 enzymes-mediated APAP bioactivation at early developmental stage through characterizing the dose-effect (0-1.6 mg/mL) and the time-course (0-72 h) of liver injury and metabolism in the AB strain and LiPan transgenic line *Tg(lfabp10a: DsRed; elaA:egfp*) expressing liver-specific fluorescent protein. APAP caused multi-organ developmental retardation and elicited dose- and time-dependent hepatotoxicity. Liver imaging revealed significant changes earlier than histological and biochemical measurements. APAP bioactivation in larval zebrafish was first confirmed by the detection of the glutathione conjugate of the reactive intermediate NAPQI (NAPQI-GSH) and subsequent mercapturate derivatives NAPQI-cysteine and NAPQI-N-acetylcysteine after even short (0.5-hour post exposure) or low (0.2 mg/mL) APAP exposure. APAP overdose impaired metabolic function, in particular sulfation, while facilitated GSH depletion and APAP sulfate excretion. Meanwhile, APAP displayed triphasic accumulation in the larvae, agreeing with fluctuating metabolic capabilities with sulfation dominating the early larval developmental stage. Most importantly, the dose-response effects and time-course of APAP accumulation and metabolism agree well with those of the liver injury development. Overall, larval zebrafish has developed mammalian-like metabolic function, enabling it an ideal model organism for high throughput screening hepatotoxicity and mechanistic study of bioactivation-based DILI.

Keywords: zebrafish model; drug-induced liver injury; acetaminophen; bioactivation; metabolic capacity; liver imaging

Abbreviations

ALT: alanine transaminase; APAP: acetaminophen; APAP-d_4, acetaminophen-d_4; APAP-Gluc: acetaminophen-glucuronide; APAP-Sulf: acetaminophen-sulfate; AST: aspartate transaminase; DILI: drug-induced liver injury; dpf: day post-fertilization; GSH: glutathione; GSTs: glutathione S-transferases; hpe: hour post-exposure; lfabp: liver fatty acid binding protein; NAPQI: *N*-acetyl-*p*-benzoquinone imine; NAPQI-Cys: NAPQI-Cysteine; NAPQI-GSH: NAPQI-Glutathione; NAPQI-NAC: NAPQI-N-acetylcysteine; SOD: superoxidase dismutase; SULT: sulfotransferases; UGTs: uridine 5'-diphospho-glucuronosyltransferases.

1. Introduction

In the past decades, zebrafish (*Danio rerio*) have emerged as a pre-eminent model organism with wide applications in drug-induced liver injury (DILI). The transparent body of larval zebrafish allows dynamic monitoring of liver injury using imaging techniques which has been developed for studying hepatotoxicity of several xenobiotics, such as APAP, isoniazid and pyrazinamide (Zhang et al. 2014). Meanwhile, metabolic studies indicate the versatile metabolic capacity of zebrafish and the orthologous relationship between zebrafish and human on main drug metabolizing enzymes, including CYPs, sulfotransferases (SULTs), uridine 5'-diphospho-glucuronosyltransferases (UGTs) and glutathione S-transferases (GSTs) (de Souza Anselmo et al. 2018). However, so far, most studies investigated the temporal and spatial expression profiles, especially the CYP system, at mRNA levels (Loerracher and Braunbeck 2021). All isozymes display fluctuating expression patterns with controversial observations been reported by different groups and so far, functional data are not available to most isoforms, making it difficult to conclude the xenobiotic biotransformation capacities of zebrafish larvae. Indeed, zebrafish could catalyze metabolism of various drugs mediated by distinct CYP isoforms in human, such as testosterone (hCYP3A4), phenacetin (hCYP1A2), and dextromethorphan (hCYP3A4 and hCYP2D6). (de Souza Anselmo et al. 2018). Nevertheless, there is still an ongoing debate on whether the larval zebrafish have sufficient capacity to biotransform and bioactivate xenobiotics or to a biologically relevant extent (Loerracher and Braunbeck 2021). Only a few studies have reported DILI-related metabolism, including APAP, diclofenac, tacrine and diterpenoid lactones from *Dioscorea bulbifera* tubers, in zebrafish model through detecting bioactivation-associated metabolites that have been reported in mammal (Loerracher and Braunbeck 2021; Shi et al. 2018). However, these studies were carried out either with liver subcellular preparations or in living organisms of zebrafish adult or larvae, most assessed statically (detected DILI-related metabolites at a single time point) after a very short exposure (within 4h). It is imperative to characterize the dose- and time-profiles of DILI-associated metabolism and liver injury development simultaneously in zebrafish larvae, which will shed light on the metabolic competency of larval zebrafish for specific xenobiotic biotransformation/bioactivation and eventually, the outcomes of toxicological studies.

Acetaminophen (APAP) is the most commonly used compound for evaluating the experimental models of DILI, especially those involving bioactivation-mediated mechanisms. Within its therapeutic dose range, APAP mainly undergoes glucuronidation (APAP-glucuronide, 52-57% of urinary metabolites) and sulfation (APAP-sulfate, 30-44% of urinary metabolites). CYP-mediated phase I reaction of APAP is minor and generates the reactive metabolite *N*-acetyl-*p*-benzoquinone imine (NAPQI), which is further detoxified by glutathione conjugation (NAPQI-glutathione, NAPQI-GSH) and ultimately excreted as cysteine and mercapturic acid conjugates NAPQI-cysteine (NAPQI-Cys) and NAPQI-N-acetylcysteine (NAPQI-NAC). With dose escalation, these detoxification pathways are gradually saturated accompanied with dramatic depletion of GSH, leading to accumulation of NAPQI which covalently binds to cellular proteins and DNA and thus causes hepatotoxicity (Mazaleuskaya et al. 2015). APAP could induce dose-dependent hepatotoxicity in larval zebrafish at very early life stage (3 hours post-fertilization) at very low exposures (0.0025~0.025 mg/mL) (Zhang et al. 2014). Sulfation and glucuronidation were also determined to be the main metabolic pathways of APAP in zebrafish larvae (3~5 days post-fertilization, dpf) exposed shortly (within 4h) to a non-toxic dose (1 mM) (Van Wijk et al. 2019). However, the bioactivation pathway of APAP in zebrafish was scarcely addressed, except for the detection of NAPQI-GSH adduct in the *in vitro* incubates of liver microsomes from adult zebrafish (Chng et al. 2012). However, it is still unclear whether APAP undergoes similar metabolic pathways and cause hepatotoxicity via the same bioactivation mechanism as reported in mammals.

Therefore, in the present study, APAP-induced liver injury and metabolism (bioactivation and phase II biotransformation pathways) in larval zebrafish were characterized in a dose escalation study and a time-course study using the wild-type (AB strain) and the LiPan transgenic fish line *Tg(lfabp10a: DsRed; elaA:egfp)* which has constitutive expression of DsRed fluorescent protein (RFP) in the liver. Regulated by liver fatty acid binding protein gene, the liver specific RFP expression can visualize and quantify hepatocytes death and retarded liver development through the reductions of liver fluorescence intensity and area (Zhang et al. 2014). Live fluorescence imaging of liver injury was compared with conventional measurements including morphological changes, histopathological analysis and biochemical indices (ALT, AST and SOD). The impact of APAP overdose on metabolic function in the

larvae was determined by measuring the mRNA expressions of main metabolizing enzymes, including *cyps* (*cyp1a1*, *1b1*, *1c1* and *3a65*), *ugts* (*ugt1a1*, *1a3*, *1a7* and *1b1*) and *sults* (*sult1 st1* and *st2* and *sult3 st1*) and the phase II conjugation (sulfation and glucuronidation) of the flavonoid compound daidzein.

2. Materials and Methods

2.1. Materials

APAP (purity≥99.0%) and tricaine methanesulfonate were purchased from Sigma-Aldrich Chemical Co. (St Louis, MO, USA). Acetaminophen-d_4 (APAP-d_4, purity≥98%), 4-acetamidophenyl-β-D-glucuronide (APAP-Gluc, purity≥98%), 4-acetaminophen sulfate (APAP-Sulf, purity≥98%), 3-(Glutathion-S-yl) acetaminophen disodium salt (NAPQI-GSH, purity≥95%), 3-cysteinyl acetaminophen trifluoroacetic acid salt (NAPQI-Cys, purity≥95%), 3-(N-acetyl-L-cystein-S-yl) acetaminophen (NAPQI-NAC, purity≥96%) were purchased from Toronto Research Chemicals Inc. (Ontario, Canada). Daidzein (≥98%) was purchased from Yuanye Bio-Technology Co., Ltd. (Shanghai, China).

2.2. Zebrafish maintenance

The wild type (AB strain) and transgenic line *Tg(lfabp10a: DsRed; elaA:egfp)* were supplied by the zebrafish core facility of Faculty of Health Science at University of Macau (Macao, China). The adult fish were maintained in ZebTEC zebrafish housing system (28°C; pH 7.3; conductivity, 400 μS/cm; 14/10 light/dark cycle) with Tritone automatic feeding system (Tecniplast, Buguggiate, Italy). Once collected from natural spawning, the embryos were reared at room temperature of 28.5±0.5°C. The dead embryos were removed and incubated water was changed daily prior to experiments. All animal experiments followed the protocol (Ref. no.: UMARE-043-2019) approved by the Research Ethics Panel of University of Macau.

2.3. Toxicological analysis of zebrafish larvae exposed to APAP

2.3.1. APAP treatment

Transgenic zebrafish larvae (3 dpf) were either treated with a series concentration of APAP within 0-1.6 mg/mL for 72 h to determine dose-response effect or exposed to 0.8mg/mL APAP for different time intervals up to 72 h to characterize the dynamics of liver injury development. Twenty larvae were immersed in 1mL drug solution for each group in dose-escalation study, while fifteen larvae were immersed in 0.6 mL solution for each predetermined time interval in time-course study. To terminate the experiment, the larvae were anesthetized by tricaine methanesulfonate (100 mg/L) solution followed by toxicological assessment (including mortality, morphology and liver histology) and liver fluorescence imaging. To determine the

dynamic changes of biochemical markers, sixty larvae were immersed in 3 mL solution and homogenized at the indicated time points for biochemical assay.

2.3.2. Morphological assessment

At the end of APAP treatment, the survivors were counted and then anesthetized for morphological assessment of liver, intestine, yolk, pericardium, and swim bladder according to Brannen's report (Brannen et al. 2010). Body length and the typical phenotypes of malformation, including uninflated swim bladder, darkened intestinal region, delayed yolk retention and pericardial edema, were recorded.

2.3.3. Liver histological analysis

Whole larva was fixed in Bouin's solution (5% acetic acid, 9% formaldehyde and 0.9% picric acid in water) and then dehydrated and infiltrated overnight using Leica ASP6025 S Automatic Vacuum Tissue Processor (Wetzlar, Germany). Afterwards, the larvae were embedded by paraffin wax for sectioning (6μm thickness) and then subjected to hematoxylin and eosin (H&E) staining. The images were captured by an Olympus IX73 inverted microscope in bright field.

2.3.4. Liver fluorescence imaging

The larvae were imaged by Olympus IX73 inverted microscope or Olympus IX81 inverted microscope with the X-Cite 120Q lamp illumination (Waltham, MA, USA) as fluorescent light source. All images were captured at the right lateral region of larvae with constant exposure time (2 ms). ImageJ software (National Institutes of Health, Bethesda) was used to determine the total intensity, mean intensity and cross-sectional area of liver fluorescence.

2.3.5. Biochemical assays

After being anesthetized and washed carefully, the larvae were homogenized with 200 μL cold normal saline followed by centrifugation (12, 000 g, 10 min, 4℃). ALT, AST and SOD activities in the resultant supernatants were determined using the commercial kits (Nanjing Jiancheng Biotechnology Institute, Nanjing, China). Meanwhile, the protein contents in the supernatants were determined using BCA protein assay kit (Beyotime Biotechnology Co., Shanghai, China).

2.4. Metabolism study of APAP in zebrafish larvae

2.4.1. APAP treatment

Wild type zebrafish larvae (3 dpf) were either treated with APAP within 0-1.6 mg/mL for 24 h to determine the dose effects or exposed to 0.8 mg/mL APAP for different time intervals up to 48 h to study the time-course of APAP metabolism. In each treatment group, 20 larvae were immersed in 1mL drug solution. After exposure, both larvae and the culture medium were collected and prepared for quantitative or qualitative analysis using liquid chromatography tandem mass spectrometry (LC-MS/MS) **(Supplementary material I)**. The larvae incubated in APAP-free medium served as the blank control, while larva-free medium containing APAP alone was performed in parallel to exclude the possibility of chemical degradation of APAP under the cultured conditions.

2.4.2. Sample preparation

After being anesthetized and washed carefully, the larvae were homogenized with 400 μL methanol/water (50/50, v/v) containing 1μg/mL APAP-d_4 as the internal standard (IS). The homogenates were centrifuged twice at 20,000 g and 4℃ for 10 min and the supernatants were subject to LC-MS/MS analysis of APAP and its metabolites. Meanwhile, the incubation medium (400 μL) was spiked with the equal volume of 2μg/mL APAP-d_4 and then directly injected for LC-MS/MS analysis.

2.5. The effects of APAP exposure on expression and function of drug-metabolizing enzymes in zebrafish larvae

2.5.1 qRT-PCR analysis of drug-metabolizing enzymes genes

The wild type zebrafish larvae (3 dpf, 40 larvae in each group) were treated with a series concentration of APAP for 24h and then anesthetized with tricaine as described in Section 2.4.1. Total RNA was extracted with TRIzol reagent (Thermo Fisher Scientific, USA) according to the manufacturer's instructions before being converted to cDNA with PrimeScript™ RT reagent kit (Takara, Japan). The cDNAs were analyzed on Bio-Rad CFX96 Real-Time System using an SYBR® Premix Ex Taq™ II (Takara, Japan). The mRNA expressions of main drug metabolizing enzymes of zebrafish larvae were determined in triplicates with the primer sequences detailed in **Supplementary material II**. The cycle threshold (CT) values for the target genes and the 18S rRNA reference gene in all samples were obtained and then the relative gene expression differences were analyzed using the $2^{-\Delta\Delta CT}$ method.

2.5.2 The conjugation of daidzein in zebrafish larvae exposed to APAP

To further determine the impact of APAP exposure on sulfation and glucuronidation, the larvae (3 dpf, 20 larvae per group) were first exposed to APAP (0.4, 0.8 and 1.2 mg/mL) for 24 h, respectively, rinsed three times, and then transferred into 1mL daidzein solution (50 μM). After 3h incubation, larvae were collected and homogenized with 200 μL methanol/water (50/50, v/v), followed by centrifugation (20, 000 g, 10 min, 4℃) twice to obtain supernatants. The culture medium was collected and spiked with equal volume of methanol. The samples obtained were subjected to LC-MS/MS analysis to determine the formations of phase II conjugates of daidzein, including two mono-glucuronides (M1 and M2) and one mono-sulfate (M3) conjugates **(Supplementary material I)**.

2.6. Statistical Analysis

Data are expressed as means ± standard deviation. One-way analysis of variance (ANOVA) between groups was conducted by SPSS software (SPSS, Inc., Chicago, IL, USA) using Dunnett test or Tukey's test for post hoc comparisons. p value < 0.05 was considered statistically significant unless otherwise specified. Graphs were plotted with GraphPad prism 8 software.

3. Results

3.1. APAP caused dose-dependent multi-organ toxicity to zebrafish larvae

APAP caused severe mortality to zebrafish larvae at high concentrations tested, with 30% and 100% death at 1.4 mg/mL and 1.6 mg/mL, respectively, after 72 h exposure **(Fig. 1A)**. Meanwhile, the morphological assessment revealed obvious change in the regions of liver, intestine, swim bladder, pericardium and yolk **(Fig. 1B)**. The number of larvae with pericardial edema, darkened intestine or uninflated swim bladder increased with dose. Swim bladder was more sensitive than intestine and heart to APAP insult with 40% of the larvae maintaining uninflated phenotype at 0.4 mg/mL APAP **(Fig. 1C-D)**. Moreover, liver fluorescence imaging analysis revealed that APAP treatment significantly reduced intensity and area of liver fluorescence in a dose-dependent manner **(Fig. 1C, E)**. When normalized with the area, the mean liver fluorescence density also exhibited a dramatic reduction. Consistently, the histological analysis showed severe nuclear atrophy, eosinophilia and cytoplasmic swelling of hepatocytes as well as more compact and irregular cell arrangement **(Fig. 1F)**, suggesting that APAP induces hepatocytes necrosis and inhibits late liver development of zebrafish larvae.

3.2. Time-course of liver injury development in zebrafish larvae exposed to APAP

The morphological changes of intestine and swim bladder and liver fluorescence of zebrafish larvae were recorded at different time points after exposure to APAP at 0.8 mg/mL **(Fig. 2A)**, a level that caused significant total liver fluorescence reduction at 72 hpe without death **(Fig. 1A, E)**. APAP overdose significantly retarded larval body growth at 48 hpe and almost abrogated swim bladder inflation after 36hpe. The intestinal deformity (darken region), mainly in the foregut region, was firstly observed as early as 12 hpe and became universal with the extension of APAP exposure. The pericardial edema appeared later (36 hpe) at lower incidence rate than other morphological changes **(Fig. 2B)**. Both fluorescence area and total intensity showed significant decreases at the first time point determined (12hpe) **(Fig. 2C)**, whereas ALT and AST levels increased significantly at 48 hpe **(Fig. 2D)**. The SOD activity in untreated larvae increased with larvae development, especially after 36hpe, while that of the APAP treated group maintained with slight fluctuation **(Fig. 2D)**. Notably, the mean fluorescence intensity didn't show significant reduction in general (except at 12hpe and 72hpe, **Fig. 2C**), which is likely attributed to more compact liver cell arrangement **(Fig. 2E)**. Nevertheless, the liver

histological changes are still highly consistent with the time-course of fluorescence area and total intensity.

3.3 Metabolism of APAP in zebrafish larvae APAP and five detoxifying metabolites, including two APAP conjugates APAP-Sulf and APAP-Gluc and three conjugates of NAPQI NAPQI-NAC, NAPQI-Cys and NAPQI-GSH, were successfully detected in both larval homogenates and incubation medium with identities unambiguously assigned by comparison of their retention times and mass spectral data with those of the authentic compounds (**Supplementary material I**).

3.3.1 The effect of dose on APAP metabolism in zebrafish larvae

At 24 hpe, only a minor amount (< 0.1% of dose) of APAP was absorbed by twenty larvae from the medium as judged from the amounts of APAP appearing in larvae and the metabolites formed. As shown in **Fig. 3A**, the accumulation of APAP in the larvae showed a dose-proportional increase. Correspondingly, the conversion of APAP to the detoxifying phase II conjugates kept increasing within 0.2-1.2 mg/mL but dropped at 1.6 mg/mL of APAP. More specifically, the glucuronide dominated APAP conjugates and displayed similar increasing tendency, while APAP-Sulf formation continuously decreased slightly with dose escalation. Thus, the glucuronide/sulfate ratio increased with APAP escalation (1.2~5.4). On the other hand, the sulfate released into medium was increased with dose **(Fig. 3B)**.

NAPQI conjugation as indicated by the formation of three NAPQI conjugates reached a plateau at 0.8mg/mL and showed a slight decline at 1.6 mg/mL **(Fig. 3A)**. The NAC conjugation is the major metabolic pathway across the dose range tested. Both NAPQI-NAC and NAPQI-Cys reached maximum levels at 0.8 and 1.2 mg/mL, respectively, while the glutathione conjugate showed dose-proportional increases within 0.4-1.2 mg/mL followed by a dramatic increase at 1.6 mg/mL **(Fig. 3A-B)**.

Except for NAPQI-GSH which was only detected in the homogenates, other four conjugates, especially the sulfate conjugate, were also found in the culture media. In general, the absolute amounts of the phase II metabolites APAP-Gluc and APAP-Sulf were tens times those formed through the conjugation of the reactive metabolite. The conjugates accumulated in the larvae displayed the following descending order: glucuronide > sulfate > NAC > glutathione > cysteine **(Fig. 3B)**.

3.3.3 The time-course of APAP metabolism in zebrafish larvae

APAP could be detected in the larvae at the first time point determined (0.5hpe), and continuously increased until 24 hpe when it started reaching a plateau. Only a minor amount of APAP was consumed by the larvae even after 48 h exposure. The accumulation rates displayed a multiphasic decline with a sharp decrease within 3 hpe, a maintenance during 6-12 hpe followed by a gradual decline (12-48 hpe) **(Fig. 4A)**.

APAP-Gluc and APAP-Sulf presented as the main metabolites throughout the experimental period (3-5 dpf). In the larval homogenate, APAP-Sulf could be detected at 0.5 hpe, earlier than APAP-Gluc (1 hpe). The amounts of APAP-Sulf detected in the homogenate were higher than APAP-Gluc at the early stage of APAP exposure (till 12 hpe). Afterwards, the accumulation of APAP-Gluc rapidly increased and significantly exceeded that of APAP-Sulf with much higher accumulation rates observed at 24 hpe **(Fig. 4B)**. In the medium, although APAP-Sulf was also detectable at 0.5 hpe, it remained at low levels within 6 hpe, while displayed facilitated biphasic excretion during 6-24 hpe and 24-48 hpe. APAP-Gluc couldn't be detected in the medium until 12 hpe and then showed linear increases till the end of experiment with amounts and rates of excretion during 24-48 hpe significantly lower than those of APAP-Sulf (excretion rate 0.18 nmol/h for APAP-Gluc versus 0.47 nmol/h for APAP-Sulf) **(Fig. 4C)**. The quicker excretion likely accounts for the lower larval accumulation of APAP-Sulf **(Fig. 4B)**. The formation of both metabolites continued to increase throughout APAP exposure, with a marked elevation after 12 hpe. APAP-Sulf presented to be the most abundant metabolite formed during the early (within 6 hpe) and late (36-48 hpe) exposure period **(Fig. 4D)**. The formation rates of both metabolites fluctuated, corresponding well with the triphasic accumulation profile of APAP (**Fig. 4A**). Interestingly, the formation rate of APAP-Sulf showed a sustained elevation, of APAP-Gluc decreased after 24hpe, suggesting the decline of glucuronidation pathway **(Fig. 4D)**.

The time-course of the bioactivation pathway of APAP was determined through monitoring the formation of NAPQI-NAC, the predominant metabolite (10-20 folds of NAPQI-GSH and NAPQI-Cys) in larvae exposed to 0.8 mg/mL APAP for 24 h. In the homogenates, NAPQI-NAC was already detectable at 1hpe and showed minor generation before 12 hpe followed by a rapid accumulation by 24 hpe, and then maintained at a stable level (24-48 hpe)

(Fig. 4B). In the medium, NAPQI-NAC couldn't be detected until 12 hpe and then showed a slight increase till the end of exposure **(Fig. 4C)**. The formation of NAPQI-NAC continuously increased, although at much lower levels with fluctuating rates **(Fig. 4D)**.

4. The effects of APAP exposure on expression and function of drug-metabolizing enzymes in zebrafish larvae

The expressions of four *cyps* (*cyp*1a1, 1b1, 1c1, 3a65) were significantly inhibited by APAP at higher doses (0.4 mg/mL or above), among which *cyp1a1* expression displayed more significant decrease **(Fig. 5A)**. Similarly, APAP (0.4 mg/mL or higher) suppressed the mRNA expression of most *ugts (1a3, 1a7* and *1b1),* except for *ugt1a1* which exhibited a dose-proportional increase of mRNA expression **(Fig. 5B)**. With regard to *sults*, APAP treatment resulted in a dose-dependent elevation of *sult3 st1* and a general suppression of *sult1 st2* (≤20% of control level) cross the tested concentration range (0.2-1.6 mg/mL) **(Fig. 5C).** The mRNA expressions of *sult1st1* in the larvae showed dramatic decreases at lower APAP levels (0.2-0.4 mg/mL), while higher doses (0.8-1.6 mg/mL) showed weaker effects.

Larval exposure to APAP weakened the phase II metabolism of daidzein. Among the three daidzein conjugates detected, including two mono-glucuronide M1 and M2 and one mono-sulfate M3 **(Supplementary material I)**, all only presented in the larval homogenate but not in the culture medium. With the dose escalation of APAP, the peak area of M1 showed insignificant change and M2 gradually decreased with ~50% reduction at 1.2 mg/mL, whereas the formation of the sulfated metabolite M3 was significantly inhibited (**Fig. 5D**).

4. Discussion

In current study, low APAP consumption (< 0.1% of 0.8 mg/mL APAP absorbed by twenty larvae at 24hpe) *in vivo* **(Fig. 3A & 4A)** is adequate to cause multi-organ malformation and body growth retard and elicit liver injury in zebrafish larvae **(Fig. 1C-E & 2A-C)**. Multi-organ toxicity of APAP including intestinal injury, heart failure, pulmonary endoplasmic reticulum stress and metabolic changes has been reported in human being, mouse or rat (Chopyk et al. 2019; Kennon-McGill and McGill 2018). This is the first report of such toxicity in zebrafish larvae. The body transparency allows *in vivo* live imaging of liver injury in the larvae by determining the area and intensity of fluorescence using the transgenic line. This study firstly revealed that liver fluorescence imaging is more sensitive to APAP induced liver injury than the conventional biochemical measurements (ALT, AST and SOD).

The main NAPQI conjugates (NAPQI-GSH, NAPQI-Cys and NAPQI-NAC) were detected for the first time with NAPQI-NAC as the most abundant form **(Fig. 3A)**, suggesting that the other two metabolites are rapidly converted to NAPQI-NAC via mercapturic acid pathway. NAPQI-NAC could be detected as early as 1 hpe **(Fig. 4B)**, indicating that the larval zebrafish (3 dpf) is competent to catalyze bioactivation of APAP as well as subsequent glutathione conjugation and mercapturic acid pathway of NAPQI. More importantly, the dose and time profiles of the bioactivation pathway agreed well with the characteristics of APAP-induced liver injury. Specifically, the combined formation of all three detoxified NAPQI metabolites were saturated when APAP concentration was increased to 0.8 mg/mL, a dose that elicited significant liver injury **(Fig. 1C-E)**; the continuous rapid increase of NAPQI-NAC after 12 hpe corresponded to the liver injury development indicated by liver imaging **(Fig. 2C)**. Additionally, previous studies reported stable GSH levels and continuously increasing GSTs enzyme expression (*Gsta1*, *Gsta2*, *Gstr*, *Gstz1*, etc.) in larval zebrafish during 3~5 dpf (Tierbach et al. 2018; Timme-Laragy et al. 2013). The time profile of NAPQI-NAC formation observed in this study agrees well with the developmental expression of the redox pathways.

Sulfation and glucuronidation are the main metabolic pathways of APAP in zebrafish larvae, agreeing with the reports in mammals (Mazaleuskaya et al. 2015). APAP dose escalation resulted in gradual saturation of APAP conjugation while elicited the CYP-mediated bioactivation pathway as evidenced by the detection of three NAPQI conjugates. NAPQI-NAC

was detected later or at higher doses than that of the sulfate conjugate (1hpe versus 0.5hpe, ≥0.4 mg/mL versus ≥0.2 mg/mL) **(Fig. 4B-C)**, indicating that the phase I bioactivation of APAP is initiated later or at higher dose than its conjugation. The elimination of APAP through conjugation secondary to the bioactivation pathway (NAPQI conjugation) seems to be also saturated and/or suppressed as evidenced by the total formation of the three NAPQI conjugates with APAP dose escalation **(Fig. 3A)**. These findings agree with the previous studies with overdose of APAP in human and other mammal models (Li et al. 2021; Mazaleuskaya et al. 2015), which confirm the occurrence of similar metabolic pathway of APAP and support the rapid development of hepatic metabolic function in larval zebrafish (3dpf).

An impairment of metabolic activity in zebrafish larvae in response to high and/or long APAP exposure was evidenced by the significant decreases of mRNA levels of some isozymes genes including all tested *cyps, ugt1a3/1a7/1b1* and *sult1 st1/st2* **(Fig. 5B-C)** as well as decreased APAP sulfate formation **(Fig. 3B)** and reduced phase II conjugation (the sulfated metabolite was more significantly decreased) of daidzein in larvae pretreated by APAP **(Fig. 5D)**. The impaired metabolic activity could be the consequences of APAP-induced liver damage which could be recovered to normal during liver regeneration (Bao et al. 2021). It could not be excluded that APAP itself and/or the metabolites formed can suppress the enzyme activity or expression directly or via alternative mechanisms. It's noteworthy that the glutathione conjugate NAPQI-GSH showed a sharp elevation in larval homogenates at 1.6 mg/mL of APAP. Abnormal elevation of plasma GSTs levels have been reported in patients poisoned by APAP and correlated with APAP-induced hepatotoxicity (Beckett et al. 1985). Thus, the sharp increase of NAPQI-GSH in larvae could be attributed to elevated GSTs levels and/or the saturation or impairment of the downstream mercapturic acid pathway in response to high APAP exposure and, as a consequence, the resulted GSH depletion can explain the major liver damage and high mortality rate at 1.6 mg/mL of APAP.

APAP accumulation rate and the formation/excretion of the metabolites generally displayed multiphasic changes **(Fig. 4A)**, indicating fluctuating metabolism/excretion function at early developmental stage of larval zebrafish. This warrants further investigation. In addition, larval APAP glucuronide accumulation showed triphasic elevation with a significant increase during 12-24 hpe, while its excretion displayed a constant rate within 6-48 hpe, indicating

saturated transport of the glucuronidated metabolite. As such, the diminished formation rates of APAP-Gluc should also be resulted from saturated excretion and/or suppressed glucuronidation after APAP exposure **(Fig.4B-D)**. APAP overdose can also cause substrate inhibition on glucuronidation by human recombinant UGT1A6, UGT2B15 and liver microsomes (Mutlib et al. 2006). The excretion of APAP-Gluc and APAP-Sulf is mediated by multiple transporters (McGill and Jaeschke 2013) and patients overdosed on APAP exhibited upregulation of several transporters in livers (Barnes et al. 2007), which could serve as an adaptive mechanism for removing toxic metabolites and developing tolerance to prevent additional liver injury from APAP overdose. Sulfation dominates the phase II conjugation of APAP after short (within 6 hpe) and long (after 36 hpe) exposure **(Fig. 4D)**. Kantae and co-workers also reported a higher APAP-Sulf level (5~6 times that of APAP-Gluc) in zebrafish larvae (3 dpf) after a shorter (3 h) exposure to a much lower dose of APAP (~0.15 mg/mL) (Kantae et al. 2016). In human neonate receiving APAP, the level of sulfate metabolite was 3.5~8 times that of the glucuronide conjugate (Allegaert et al. 2005; van Lingen et al. 1999), in contrast to APAP-Gluc dominating APAP metabolism in adult human treated with a therapeutic dose of APAP (Mazaleuskaya et al. 2015). Interestingly, the formation ratio of APAP-Sulf/APAP-Gluc (1.1~2.2) throughout the experimental period (except for 24hpe) was much lower than that reported previously (APAP-Sulf/APAP-Gluc ratio 5~6) with a much shorter (3 h) and lower APAP (~0.15 mg/mL) exposure (Kantae et al. 2016). Daidzein sulfation also displayed more pronounced reduction in larvae pretreated by APAP **(Fig. 5D)**. These results suggest that sulfation is a reaction of higher affinity and lower capacity than that of glucuronidation and more susceptible to the level and the time of APAP exposure in the early developmental stage of larval zebrafish.

Even though larval zebrafish has acquired similar metabolic capability to mammals and is advantageous in offering high throughput organism-level screening, it still faces some limitations, such as the technical challenges in accurate drug dosing, predictable compound consumption by individual fish, blood sampling and sensitive analytical methods posed by the tiny body size. As such, ALT and AST levels in larval homogenates were measured in this study, instead of those in plasma/serum which are typically adopted as the indices of hepatocyte damage and also reported with adult zebrafish (5~24 months old) (Vliegenthart et al. 2014).

Similar elevation of aminotransferase activities in larval homogenates were also reported in numerous studies assessing DILI with larvae model (Li et al. 2020; McGill 2016) and our study showed good correlations between the time profiles of ALT and AST levels and the liver injury, thus should be closely associated with liver injury despite the mechanisms remaining unclear. Moreover, the extrahepatic toxicity caused by APAP poisoning is most demonstrated to be the consequences of local exposure to the reactive intermediate NAPQI (Chopyk et al. 2019; Kennon-McGill and McGill 2018), and thus might be attributed to spatiotemporal distribution of P450s, differential tissue exposures to APAP and/or its metabolites and/or systemic consequences of APAP-caused liver damage in larval zebrafish. Such knowledge in early developmental stage of zebrafish larvae is still not available. The knowledge gap in functional activity and spatiotemporal distribution of drug-metabolizing enzymes in zebrafish larvae, especially those involved in APAP metabolism (bioactivation) does not allow reasonable interpretation of pathogenesis in APAP-induced liver injury.

In conclusion, our study first systematically characterized the effects of dose and exposure time on hepatotoxicity of APAP and correlated it with the metabolism in zebrafish larvae. Hepatic fluorescence expression displayed dose- and time-dependent reduction which appeared earlier than conventional measurements of liver injury. Dose escalation resulted in elevated glucuronidation but continuously diminished sulfation of APAP, while prolonged APAP exposure caused a facilitated sulfate conjugate excretion and time-varying accumulation/metabolite formation. More importantly, the larval zebrafish demonstrates the ability of catalyzing phase I bioactivation of APAP as well as the subsequent glutathione conjugation and mercapturic acid pathway, as evidenced by the detection of the conjugates of NAPQI. The dose and time profiles of APAP accumulation and metabolism highly agree with those of the liver injury development, supporting that zebrafish larvae quickly acquire related metabolic capability which enables it an ideal model for investigating bioactivation caused DILI as well as drug screening.

FUNDING

The project is supported by the Science and Technology Development Fund, Macao S.A.R (FDCT-0098/2019/A2), the Research Fund of University of Macau (MYRG2018-00091-ICMS).

DECLARATION OF CONFLICTING INTERESTS

The authors declared no potential conflicts of interest with respect to the research, authorship, and/or publication of this article.

AUTHOR CONTRIBUTIONS

Yijia Chen: Conceptualization, Methodology, Software, Investigation, Writing-Original Draft, Data Curation. Weiyi Song: Resources, Methodology. Wei Ge: Resources, Methodology, Supervision. Ru Yan: Writing - Review & Editing, Project administration, Supervision, Funding acquisition

Figure Legends

Fig. 1 The effects of dose on liver injury in zebrafish larvae treated with APAP for 72h. **(A)** Mortality rate. **(B)** Representative malformation. L, liver; SB, swim bladder; I, intestine; Y, yolk; P, pericardium. **(C)** Representative images of morphology (upper) and liver fluorescence imaging (bottom). Scale bar=200μm. **(D)** Number of zebrafish larvae showing malformation in swim bladder, intestine and heart. **(E)** Liver fluorescence area, total intensity and mean intensity of the larvae. **(F)** Representative H&E staining images of larval liver. The liver is outlined with black dotted line, and the hepatocytes with nuclear atrophy and cytoplasmic swelling are indicated by arrows. Scale bar=5μm. Twenty larvae were assessed for each group, except for fourteen larvae used for the 1.4mg/mL group due to six deaths. Data in (E) are expressed in mean ± SD (n=20), $^{*}p < 0.05$, $^{**}p < 0.01$ versus control.

Fig. 2 The time-course of morphological changes and hepatotoxicity of zebrafish larvae in control and 0.8mg/mL APAP treatment group. (A) Representative images of morphology and liver fluorescence imaging of the larvae, scale bar=200μm. **(B-D)** The time-course of morphological changes (B), hepatic fluorescence expression (C) and liver biochemical indices (D) of the larvae. **(E)** The time-course of hepatic histological progression in the larvae. Liver is outlined with black dotted line and hepatocytes with nuclear atrophy and cytoplasmic swelling are indicated by arrows. Scale bar=5μm. At each time point, the body length and liver fluorescence expression were measured from fifteen larvae in one experiment. The swim bladder inflation, intestinal deformity and pericardial edema of fifteen larvae were determined from three independent experiments. The liver biochemical indices were measured from the homogenates of sixty larvae and the experiment was repeated three times. Data in (B-D) are expressed in mean ± SD. $^{*}p < 0.05$, $^{**}p < 0.01$ versus control.

Fig. 3 APAP accumulation and the metabolites formation in zebrafish larvae exposed to APAP for 24h. (A) The accumulation of APAP and total formation of phase II APAP conjugates and NAPQI conjugates. **(B)** The amounts of each metabolite determined in the larval homogenates and incubation medium. Homogenates of twenty zebrafish larvae and the culture media from each group were collected for analysis.

Fig. 4 The time-course of APAP accumulation and the main metabolites accumulated,

excreted and totally formed in zebrafish larvae exposed to 0.8mg/mL APAP. (A) The amount and the rate of APAP accumulation. **(B-D)** The amounts and rates of the metabolites accumulated in larvae (B), excreted into the culture medium (C) and totally formed (D). Data were determined from three independent experiments, and expressed in mean ± SD. * denotes the significant difference between the amount/rate of APAP-Sulfate and that of APAP-Glucuronide at the same time point; # denotes statistical significance between the amounts/rates of APAP-Sulfate and NAPQI-NAC, & denotes statistical significance between the amounts/rates of APAP-Glucuronide and NAPQI-NAC. $^{*,\#,\&}p < 0.05$, $^{**,\#\#,\&\&}p < 0.01$ between pairwise group.

Fig. 5 The mRNA expressions of main drug-metabolizing enzymes and phase II metabolism of daidzein in zebrafish larvae exposed to APAP for 24h. (A-C) mRNA expression levels of the main *cyp* (A), *ugt* (B) and *sult* (C) genes of zebrafish larvae. All genes measured by PCR were normalized with 18S rRNA as the reference gene. **(D)** The peak areas of the glucuronidated (M1 and M2) and the sulfated (M3) metabolites of daidzein detected in larval homogenates.

References

Allegaert K, de Hoon J, Verbesselt R, Vanhole C, Devlieger H, Tibboel D. 2005. Intra- and interindividual variability of glucuronidation of paracetamol during repeated administration of propacetamol in neonates. Acta Paediatr. 94(9):1273-1279.

Bao Y, Phan M, Zhu J, Ma X, Manautou JE, Zhong XB. 2021. Alterations of cytochrome p450-mediated drug metabolism during liver repair and regeneration after acetaminophen-induced liver injury in mice. Drug Metab Dispos. 50(5):694-703.

Barnes SN, Aleksunes LM, Augustine L, Scheffer GL, Goedken MJ, Jakowski AB, Pruimboom-Brees IM, Cherrington NJ, Manautou JE. 2007. Induction of hepatobiliary efflux transporters in acetaminophen-induced acute liver failure cases. Drug Metab Dispos. 35(10):1963-1969.

Beckett GJ, Chapman BJ, Dyson EH, Hayes JD. 1985. Plasma glutathione s-transferase measurements after paracetamol overdose: Evidence for early hepatocellular damage. Gut. 26(1):26-31.

Brannen KC, Panzica-Kelly JM, Danberry TL, Augustine-Rauch KA. 2010. Development of a zebrafish embryo teratogenicity assay and quantitative prediction model. Birth Defects Res B Dev Reprod Toxicol. 89(1):66-77.

Chng HT, Ho HK, Yap CW, Lam SH, Chan EC. 2012. An investigation of the bioactivation potential and metabolism profile of zebrafish versus human. J Biomol Screen. 17(7):974-986.

Chopyk DM, Stuart JD, Zimmerman MG, Wen J, Gumber S, Suthar MS, Thapa M, Czaja MJ, Grakoui A. 2019. Acetaminophen intoxication rapidly induces apoptosis of intestinal crypt stem cells and enhances intestinal permeability. Hepatol Commun. 3(11):1435-1449.

de Souza Anselmo C, Sardela VF, de Sousa VP, Pereira HMG. 2018. Zebrafish (danio rerio): A valuable tool for predicting the metabolism of xenobiotics in humans? Comparative biochemistry and physiology Toxicology & pharmacology : CBP. 212:34-46.

Kantae V, Krekels EH, Ordas A, Gonzalez O, van Wijk RC, Harms AC, Racz PI, van der Graaf PH, Spaink HP, Hankemeier T. 2016. Pharmacokinetic modeling of paracetamol uptake and clearance in zebrafish larvae: Expanding the allometric scale in vertebrates with five orders of magnitude. Zebrafish. 13(6):504-510.

Kennon-McGill S, McGill MR. 2018. Extrahepatic toxicity of acetaminophen: Critical evaluation of the evidence and proposed mechanisms. J Clin Transl Res. 3(3):297-310.

Li J, Chiew AL, Isbister GK, Duffull SB. 2021. Sulfate conjugation may be the key to hepatotoxicity in paracetamol overdose. Br J Clin Pharmacol. 87(5):2392-2396.

Loerracher AK, Braunbeck T. 2021. Cytochrome p450-dependent biotransformation capacities in embryonic, juvenile and adult stages of zebrafish (danio rerio)-a state-of-the-art review. Arch Toxicol. 95(7):2299-2334.

Mazaleuskaya LL, Sangkuhl K, Thorn CF, FitzGerald GA, Altman RB, Klein TE. 2015. Pharmgkb summary: Pathways of acetaminophen metabolism at the therapeutic versus toxic doses. Pharmacogenet Genomics. 25(8):416-426.

McGill MR. 2016. The past and present of serum aminotransferases and the future of liver injury biomarkers. EXCLI J. 15:817-828.

McGill MR, Jaeschke H. 2013. Metabolism and disposition of acetaminophen: Recent advances in relation to hepatotoxicity and diagnosis. Pharm Res. 30(9):2174-2187.

Mutlib AE, Goosen TC, Bauman JN, Williams JA, Kulkarni S, Kostrubsky S. 2006. Kinetics of acetaminophen glucuronidation by udp-glucuronosyltransferases 1a1, 1a6, 1a9 and 2b15. Potential implications in acetaminophen-induced hepatotoxicity. Chem Res Toxicol. 19(5):701-709.

Shi W, Ling J, Jiang LL, Zhao DS, Wang LL, Wu ZT, Li P, Wei YJ, Li HJ. 2018. Metabolism of five diterpenoid lactones from dioscorea bulbifera tubers in zebrafish. Rsc Adv. 8(14):7765-7773.

Tierbach A, Groh KJ, Schonenberger R, Schirmer K, Suter MJ. 2018. Glutathione s-transferase protein expression in different life stages of zebrafish (danio rerio). Toxicol Sci. 162(2):702-712.

Timme-Laragy AR, Goldstone JV, Imhoff BR, Stegeman JJ, Hahn ME, Hansen JM. 2013. Glutathione redox dynamics and expression of glutathione-related genes in the developing embryo. Free Radic Biol Med. 65:89-101.van Lingen RA, Deinum JT, Quak JM, Kuizenga AJ, van Dam JG, Anand KJ, Tibboel D, Okken A. 1999. Pharmacokinetics and metabolism of rectally administered paracetamol in preterm neonates. Arch Dis Child Fetal Neonatal Ed. 80(1):F59-63.

Van Wijk RC, Krekels EHJ, Kantae V, Ordas A, Kreling T, Harms AC, Hankemeier T, Spaink HP, van der Graaf PH. 2019. Mechanistic and quantitative understanding of pharmacokinetics in zebrafish larvae through nanoscale blood sampling and metabolite modeling of paracetamol. J Pharmacol Exp Ther. 371(1):15-24.

Vliegenthart AD, Starkey Lewis P, Tucker CS, Del Pozo J, Rider S, Antoine DJ, Dubost V, Westphal M, Moulin P, Bailey MA et al. 2014. Retro-orbital blood acquisition facilitates circulating microrna measurement in zebrafish with paracetamol hepatotoxicity. Zebrafish. 11(3):219-226.

Zhang XY, Li CX, Gong ZY. 2014. Development of a convenient in vivo hepatotoxin assay using a transgenic zebrafish line with liver-specific dsred expression. Plos One. 9(3).

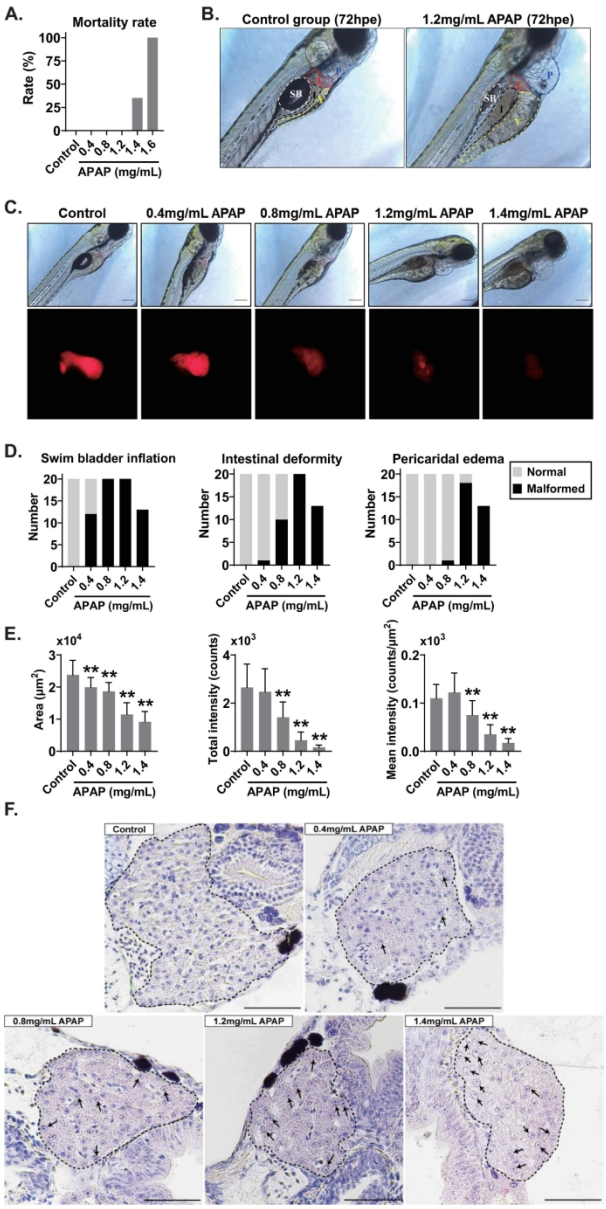

Fig 1

136x272mm (300 x 300 DPI)

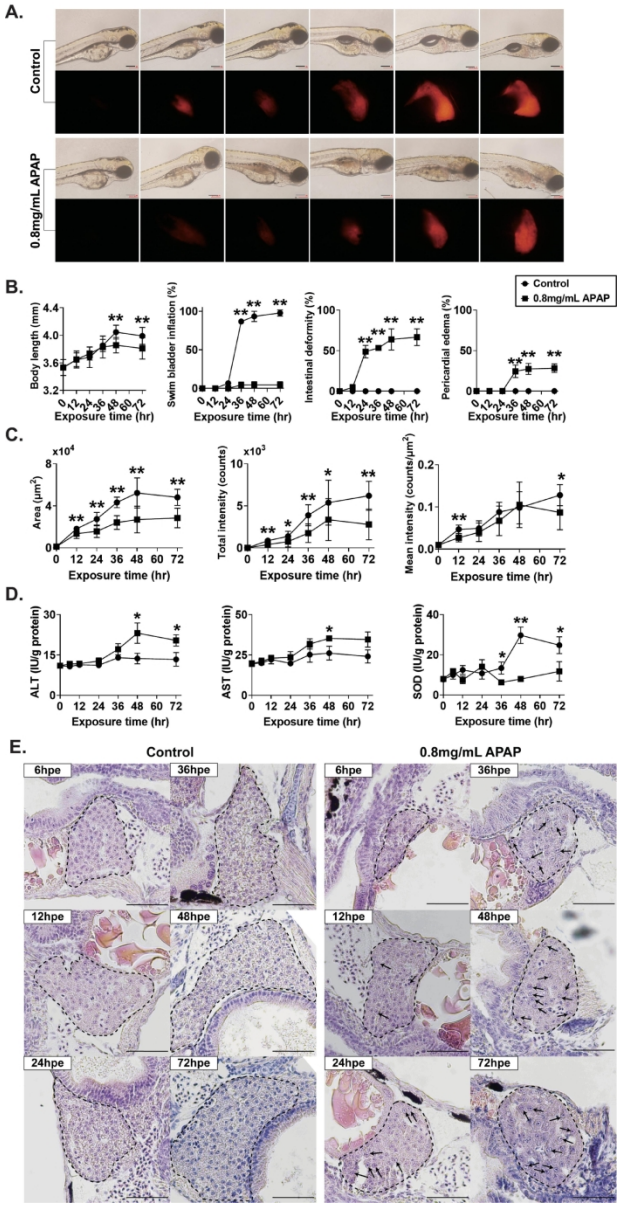

Fig 2

138x271mm (300 x 300 DPI)

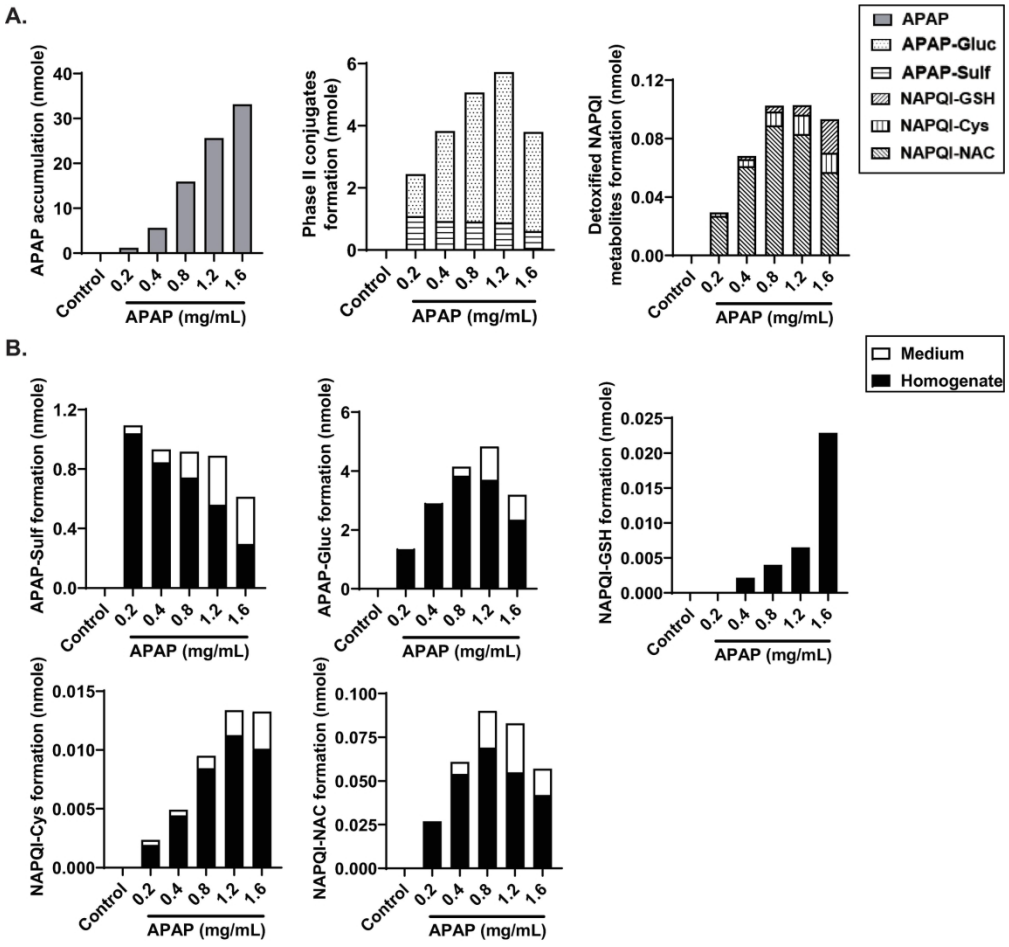

Fig 3

186x177mm (300 x 300 DPI)

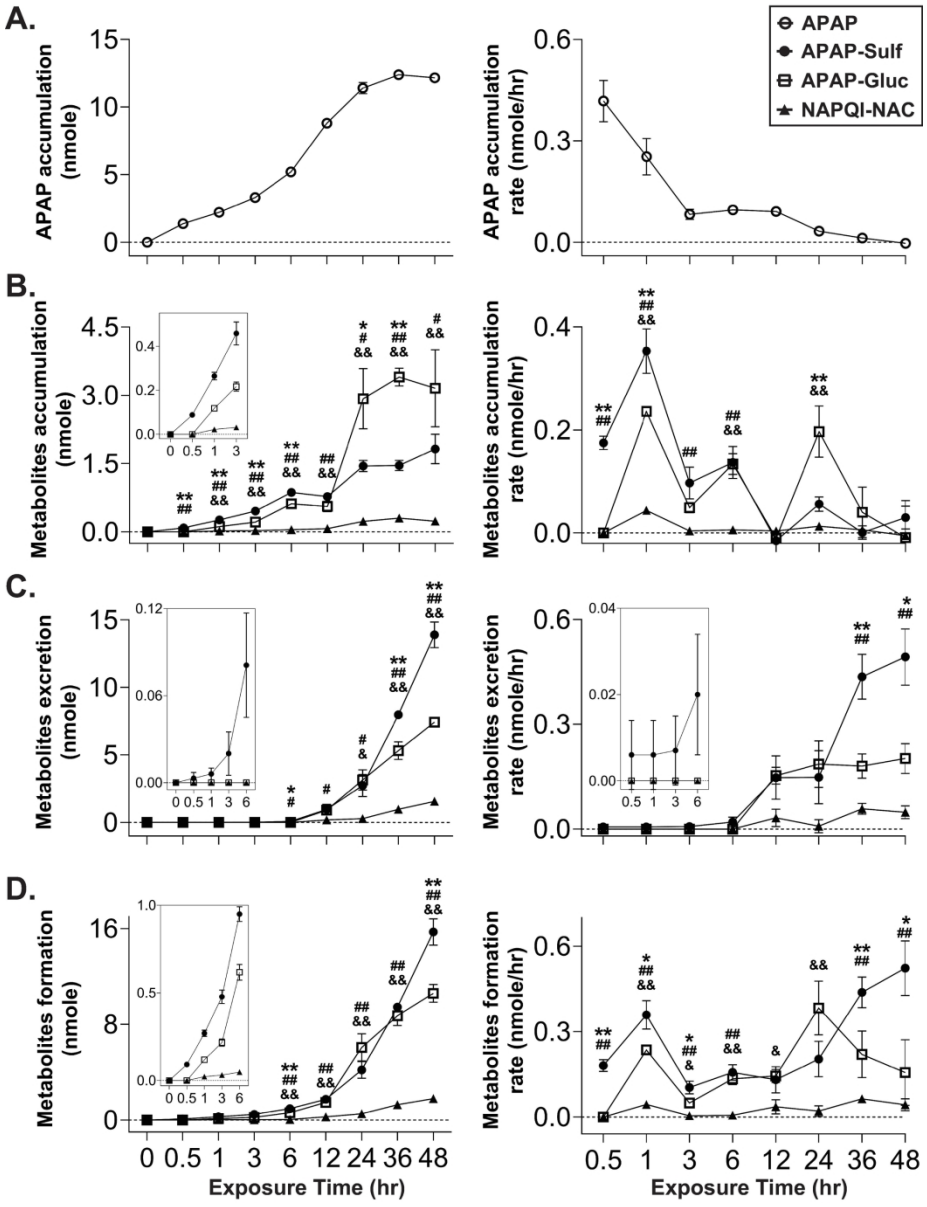

Fig 4

194x253mm (300 x 300 DPI)

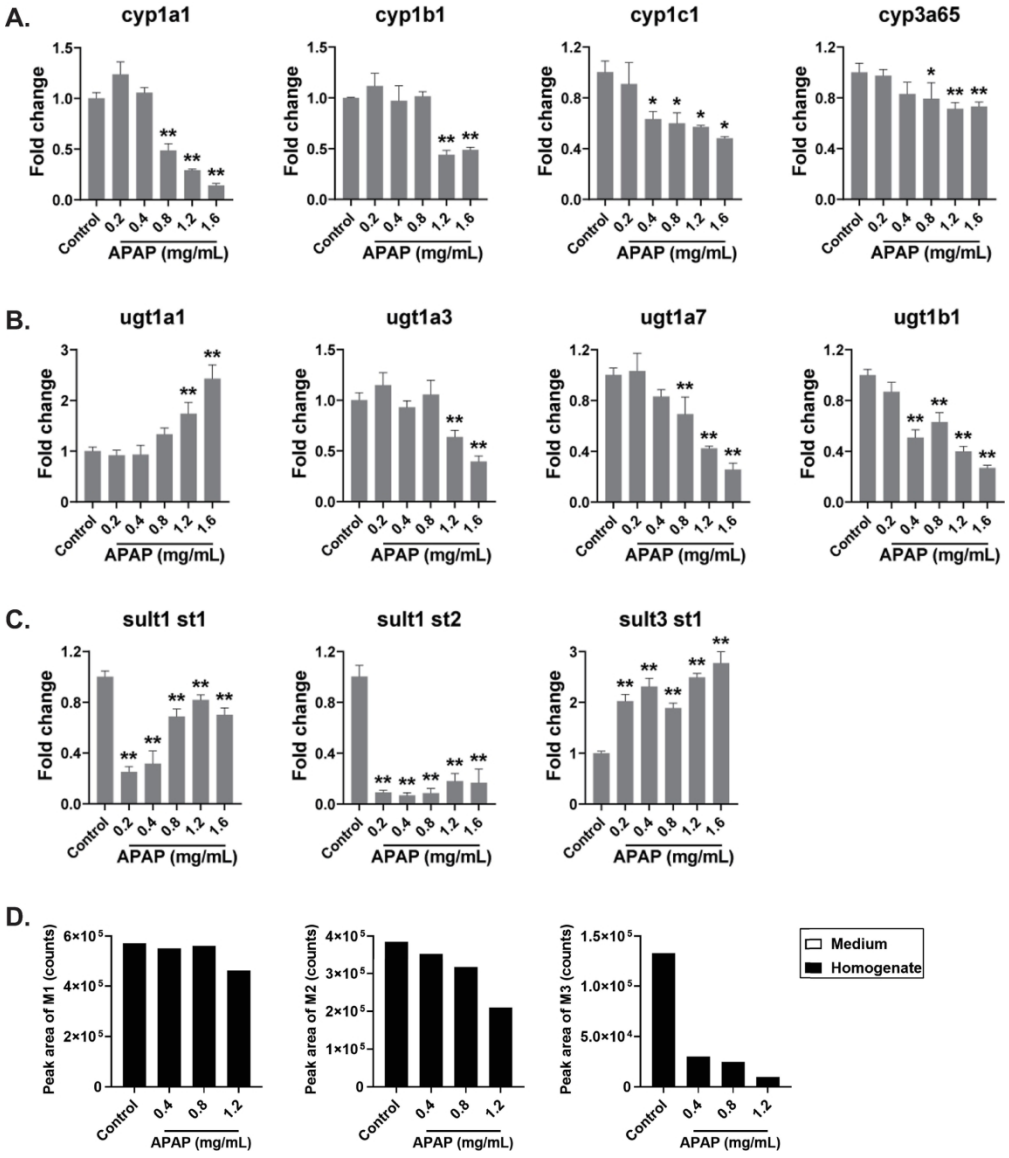

Fig 5

189x217mm (300 x 300 DPI)

Metabolic competency of larval zebrafish in drug-induced liver injury: a case study of acetaminophen poisoning

Yijia Chen[*], Weiyi Song[†], Wei Ge[†,1], Ru Yan[*,‡,1]

[*]State Key Laboratory of Quality Research in Chinese Medicine, Institute of Chinese Medical Sciences, University of Macau, Taipa, Macao, China

[†]Center of Reproduction, Development and Aging (CRDA), Faculty of Health Sciences, University of Macau, Taipa, Macau, China

[‡]Zhuhai UM Science & Technology Research Institute, Zhuhai, 519080, China

[1]To whom correspondence should be addressed at Institute of Chinese Medical Sciences, State Key Laboratory of Quality Research in Chinese Medicine, University of Macau, Research Building N22, Taipa, Macau, China. Email: ruyan@um.edu.mo. https://orcid.org/0000-0001-6268-360X.